G3, 2021, 11(5), jkab091
DOI: 10.1093/g3journal/jkab091
Advance Access Publication Date: 23 March 2021
Investigation

Chi-miR-370-3p regulates hair follicle morphogenesis of Inner Mongolian cashmere goats

Erhan Hai,[1,†] Wenjing Han,[2,†] Zhihong Wu,[1,3,†] Rong Ma,[1] Fangzheng Shang,[1] Min Wang,[1] Lili Liang,[1] Youjun Rong,[1] Jianfeng Pan,[1] Zhiying Wang,[1] Ruijun Wang,[1] Rui Su,[1] Yanhong Zhao,[1] Zhihong Liu,[1] Zhixin Wang,[1] Jinquan Li,[4,5,6,*] and Yanjun Zhang[1,*]

[1]College of Animal Science, Inner Mongolia Agricultural University, Hohhot 010018, Inner Mongolia, China
[2]College of Chemistry and Life Science, Chifeng University, Chifeng 024000, Inner Mongolia, China
[3]Department of Agriculture, College of Hetao, Bayannur 015000, Inner Mongolia, China
[4]Key Laboratory of Animal Genetics, Breeding and Reproduction, Hohhot 010018, Inner Mongolia, China
[5]Key Laboratory of Mutton Sheep Genetics and Breeding, Ministry of Agriculture, Hohhot 010018, Inner Mongolia, China
[6]Engineering Research Center for Goat Genetics and Breeding, Hohhot 010018, Inner Mongolia, China
[†]These authors contributed equally to this work.

*Corresponding author: College of Animal Science, Inner Mongolia Agricultural University, Hohhot 010018, Inner Mongolia, China. lijq@imau.edu.cn (J.L.); imauzyj@imau.edu.cn; imauzyj@163.com (Y.Z.)

Abstract

MicroRNAs (miRNAs), a class of 22 nucleotide (nt) noncoding RNAs, negatively regulate mRNA posttranscriptional modification in various biological processes. Morphogenesis of skin hair follicles in cashmere goats is a dynamic process involving many key signaling molecules, but the associated cellular biological mechanisms induced by these key signaling molecules have not been reported. In this study, differential expression, bioinformatics, and Gene Ontology/Kyoto Encyclopedia of Genes and Genomes enrichment analyses were performed on miRNA expression profiles of Inner Mongolian cashmere goats at 45, 55, and 65 days during the fetal period, and chi-miR-370-3p was identified and investigated further. Real-time fluorescence quantification (qRT-PCR), dual luciferase reporting, and Western blotting results showed that *transforming growth factor beta receptor 2* (*TGF-βR2*) and *fibroblast growth factor receptor 2* (*FGFR2*) were the target genes of chi-miR-370-3p. Chi-miR-370-3p also regulated the expression of *TGF-βR2* and *FGFR2* at mRNA and protein levels in epithelial cells and dermal fibroblasts. DNA staining, Cell Counting Kit-8, and fluorescein-labelled Annexin V results showed that chi-miR-370-3p inhibited the proliferation of epithelial cells and fibroblasts but had no effect on apoptosis. Cell scratch test results showed that chi-miR-370-3p promoted the migration of epithelial cells and fibroblasts. Chi-miR-370-3p inhibits the proliferation of epithelial cells and fibroblasts by targeting *TGF-βR2* and *FGFR2*, thereby improving cell migration ability and ultimately regulating the fate of epithelial cells and dermal fibroblasts to develop the placode and dermal condensate, inducing hair follicle morphogenesis.

Keywords: chi-miR-370-3p; hair follicle; cashmere goat; cell proliferation; cell migration

Introduction

Goats are one of the earliest domesticated livestock species. Due to their strong adaptability to the environment, they can inhabit extreme environments such as the Gobi Desert and the Mongolian Plateau, and they are now distributed worldwide (Han *et al.* 2020). China has the largest number of goats and is the world's largest cashmere exporter, due to valuable cashmere goat species resources, especially Inner Mongolian and Liaoning cashmere goats (Zhang *et al.* 2019). Cashmere is a high-grade textile raw material, known as "soft gold," and with the rapid development of textile and garment industries, the quality requirements for cashmere are becoming stricter. Thus, the selection and development of excellent cashmere goat breeds are important (Shamsaddini-Bafti *et al.* 2012).

The skin and hair follicle traits of cashmere goats have a direct effect on the yield and quality of wool. Understanding the structure, morphogenesis and development of skin hair follicles, and the functions of related genes is, therefore, of great significance to the breeding of cashmere goats. Most previous studies on cashmere goat skin hair follicles have focused on periodic changes in hair follicles, while relatively few studies on placode (PC) and dermal condensate (DC) formation have been reported. By 45 days during the fetal period in cashmere goats, the skin forms a complete epidermal structure; by 55 days, epithelial cells form PC and begin to induce dermal fibroblasts to form DC; and by 65 days, PC and DC are fully formed and downgrew (Wu *et al.* 2020a). The morphogenesis of hair follicles in the embryonic period involves gradual signaling between the epidermis, dermis, and related tissues. For example, *ectodysplasin A*, *FGF20*, and *bone morphogenetic protein 4* are expressed in the initial stages of hair follicle morphogenesis and are located on the PC, suggesting that they play an important role in PC formation in cashmere goats (Wang *et al.* 2020; Wu *et al.* 2020b). Fetal skin RNA sequencing

Received: February 18, 2021. **Accepted:** March 15, 2021

(RNA-seq) results from Inner Mongolian cashmere goats (Han *et al.* 2020; Wu *et al.* 2020a; Zhang *et al.* 2019) and Shanbei cashmere goats (Gao *et al.* 2016; Wang *et al.* 2020) showed that the Wingless-type MMTV integration site family member (WNT) and mitogen-activated protein kinase signaling pathways play an important role in the induction, differentiation, and maturation of cashmere goat hair follicles.

The genetic regulation of fetal hair follicles in cashmere goats is relatively clear, but the cellular biological mechanisms of the key signaling molecules remain unknown. Although epithelial cells and dermal fibroblasts are crucial in hair follicle development (Epstein *et al.* 1999), the cellular mechanisms through which epithelial cells and dermal fibroblasts form hair follicles have not been reported. In recent years, with the development of *in vitro* imaging technologies and single-cell sequencing, researchers have confirmed that cell migration is the main cellular mechanism of epithelial cell PC formation (Ahtiainen *et al.* 2014) and dermal fibroblast DC formation (Mok *et al.* 2019) in mice. However, there are no relevant reports on cashmere goats.

Micro-RNAs (miRNAs) are a class of endogenous noncoding RNAs 20–25 nucleotides (nt) in length with regulatory functions in eukaryotes. Mature miRNAs are produced from longer primary transcripts by a series of nuclease shearing and processing steps, then assembled into an RNA-induced silencing complex. The target mRNA is identified by complementary base pairing, and translation of the target mRNA is suppressed according to the degree of complementarity (Gebert and Macrae 2019; Suzuki *et al.* 2015). Since the discovery of miRNAs in the early 1990s (Bruce *et al.* 1993; Lee et al. 1993), thousands of miRNAs have been identified in animals and plants (Kozomara et al. 2019). Studies have shown that miRNAs affect several major biological pathways by regulating most protein-coding genes (Bartel 2018; Liu *et al.* 2018). They are widely distributed gene expression regulators and are important in the development of skin hair follicles (Andl *et al.* 2006; Yi *et al.* 2006, 2009). They regulate hair follicle development-related genes, thereby altering cell phenotype and the fate of epithelial cells, fibroblasts, dermal papilla cells, and hair follicle stem cells. Hair follicle development and morphological changes are largely governed by these cells (Ahmed *et al.* 2011, 2014; Amelio *et al.* 2013; Wu *et al.* 2021).

To explore the role of miRNAs in the formation of PC and DC, we conducted differential expression analysis of miRNA transcriptome data obtained during the early stages of fetal morphogenesis in Inner Mongolian cashmere goats. We identified chi-miR-370-3p and subsequently explored regulatory relationships between chi-miR-370-3p and *fibroblast growth factor receptor 2* (*FGFR2*) and *transforming growth factor beta receptor 2* (*TGF-βR2*), as well as the effects on the migration, cell cycle, proliferation, and apoptosis of fetal epithelial cells and dermal fibroblasts. Our findings help to explain the regulatory mechanisms of miRNAs in PC and DC formation.

Materials and methods

Animals

Samples were obtained from Inner Mongolia Jinlai Animal Husbandry Technology Co., Ltd. (Hohhot, Inner Mongolia). The environment in the farm met the relevant requirements of the experimental facilities in the Chinese National Standard "Experimental Animal Environment and Facilities" (GB14925-2010). Health status, pathogenic microorganism infections, and zoonotic infections were monitored to ensure animal safety. Mating of experimental animals was completed in the natural state of estrus. We used Graphpad Prism 9.0 to visualize the data.

Differential expression of miRNAs

In a previous study, our team sequenced miRNAs in 21 skin samples from Inner Mongolian cashmere goats during seven prenatal periods (45–135 days) (Han *et al.* 2020) (Supplementary Table S1). On this basis, the present study focused on the three periods from 45–65 days. Transcripts per million (TPM) was used to normalize miRNA expression using the formula: TPM = (actual miRNA count/total count of clean reads) $\times 10^6$. The R software package "edgeR" (http://www.bioconductor.org/packages/release/bioc/html/edgeR.html) was used to determine significant differences in expression levels between the two groups of samples. The screening criteria for miRNA differences were an expression level change of more than 1.5-fold and $P < 0.05$. We used Graphpad Prism 9.0 to visualize the data.

Key miRNA screening

TargetScan (http://www.targetscan.org/vert_71/) and MiRanda (http://www.microrna.org/microrna/home.do) were used to predict the potential target genes of miRNAs. G: Profiler (http://biit.cs.ut.ee/gprofiler/gost) was used to investigate the statistical enrichment of candidate target genes in Kyoto Encyclopedia of Genes and Genomes (KEGG) pathways and Gene Ontology (GO) functions. KEGG pathways were analyzed using the KEGG database (http://www.KEGG.jp) and GO functional enrichment analysis was carried out using the GO database (http://geneontology.org/). We used Graphpad Prism 9.0 to visualize the data.

Real-time quantitative PCR

Total RNA was isolated from skin samples and cells using TRIzol (Invitrogen, China), reverse-transcribed into cDNA using a PrimeScript Reagent Kit (Takara, China), real-time quantitative PCR (qRT-PCR) was performed using a Fluorescence Quantitative PCR Kit (Takara), and mRNA expression levels were calculated using the $2^{-\Delta\Delta CT}$ method (Schmittgen and Livak 2008). For qRT-PCR of miRNAs, RNA was reverse-transcribed into cDNA using a Bulge-Loop miRNA qRT-PCR Starter Kit (RiboBio, China), and qRT-PCR was performed using a Bulge-Loop miRNA qRT-PCR Starter Kit (RiboBio). The Pearson correlation coefficient was used to calculate the correlation coefficient between miRNAs and target genes, and two-tailed *t*-tests were employed to compare the results of the different groups. Data are presented as the mean ± standard error of the mean (SEM). We used Graphpad Prism 9.0 to visualize the data.

Dual luciferase reporter gene assay

Primers for amplifying target genes and target gene 3′-untranslated regions (UTRs) were designed based on gene sequences in GenBank, and 3′-UTR sequences were amplified by PCR using cashmere goat genomic DNA as template. PCR products were cloned into the pSI-checK2 dual-luciferase reporter gene vector (Hanheng, China) to construct the wild-type plasmid. The target sequence of chi-miR-370-3p in *FGFR2* and *TGF-βR2* genes was mutated to construct mutant plasmids. Finally, expression of the luciferase reporter was measured, and the target sites of miRNAs in the transfected 3′-UTRs were analyzed. The plasmid and chi-miR-370-3p mimics were synthesized by Shanghai Hanheng Biotechnology Co., Ltd., Shanghai, China. Two-tailed *t*-tests were used to compare the results of the different group, and data are presented as the mean ± SEM. We used Graphpad Prism 9.0 to visualize the data.

Cell culture and transfection

Cell culture and transfection were performed as described in a previous study (Wu et al. 2021). Lentivirus-mediated chi-miR-370-3p interference and overexpression plasmids were prepared by Shanghai Hanheng Biotechnology Co., Ltd. Animals were divided into negative control (NC), HBLV-chi-miR-370-3p-sponge-ZsGreen-PURO (chi-miR-370-3p [lo]), and HBLV-chi-miR-130b-3p-ZsGreen-PURO (chi-miR-370-3p [hi]) groups. We used Graphpad Prism 9.0 to visualize the data.

Western blotting

Total protein extraction and Western blotting were performed as described in a previous study (Wu et al. 2021). Antibodies were as follows: rabbit polyclonal antibody against FGFR2 (AF0159; Affinity, China), rabbit polyclonal antibody against TGF-βR2 (AF5449; Affinity), mouse monoclonal antibody against β-actin, horseradish peroxidase (HRP)-conjugated goat anti-rabbit second antibody (BA1054; BOSTER, China), and HRP-conjugated goat anti-mouse second antibody (BA1051; BOSTER). All antibodies were diluted 1:1000. Two-tailed *t*-tests were used to compare the results of different groups, and data are presented as the mean ± SEM. We used Graphpad Prism 9.0 to visualize the data.

DNA staining

Determination of the cell cycle by the DNA Content Quantitation Method (Solarbio, China) was performed according to the manufacturer's instructions. Single-cell suspensions were prepared at a concentration of 10^5/mL, and 1 mL samples were centrifuged, the supernatant was discarded, and cells were mixed with 500 μL of 70% precooled ethanol for fixation for 24 h, stored at 4°C, and the fixing solution was washed with phosphate-buffered saline (PBS) before staining; 100 L RNase A solution was added to the cell precipitation, the cells were resuspended, and bathed at 37°C for 30 min. Then 400 L propidium iodide (PI) staining solution was added to mix well and incubated at 4°C in dark for 30 min. The red fluorescence at the excitation wavelength of 488 nm was recorded. Proliferation index = (S + G2/M)/(G0/G1 + S + G2/M) %. Two-tailed *t*-tests were used to compare the results of the different groups, and data are presented as the mean ± SEM. We used Graphpad Prism 9.0 to visualize the data.

Cell Counting Kit-8

Cell proliferation was measured by the Cell Counting Kit-8 (CCK-8) assay (Tiangen, China) according to the manufacturer's instructions. Cells were seeded in 96-well plates and the optical density of each well was determined at 490 nm. Two-tailed *t*-tests were used to compare the results of different groups, and data are presented as the mean ± SEM. We used Graphpad Prism 9.0 to visualize the data.

Fluorescein-labelled Annexin V

Determination of apoptosis was performed using an Annexin V-FITC Apoptosis Detection Kit I (Lake Franklin, New Jersey, USA) according to the manufacturer's instructions. Single-cell suspensions were prepared at a concentration of 10^5/mL, and 1 mL was centrifuged, the supernatant was discarded, and 200 μL of 1× binding buffer was added. Next, 5 μL of Annexin V-FITC was added and incubated in the dark for 15 min, followed by 5 μL of PI and a further incubation in the dark for 5 min. Finally, 200 μL of 1× binding buffer was added before flow cytometry detection, and the proportion of apoptotic cells was calculated using the formula: apoptosis = (early apoptotic cells + late apoptotic cells)/total cells. Two-tailed *t*-tests were used to compare the results of different groups, and data are presented as the mean ± SEM. We used Graphpad Prism 9.0 to visualize the data.

Cell scratch test

Firstly, a marker pen was used to draw horizontal lines uniformly (every 0.5–1 cm) across a six-well plate. Approximately five cells were added to each well (adjusted according to the growth speed of cells; inoculation was based on the cell fusion rate reaching 100% after overnight). The next day, with the head of the gun perpendicular to the cell plane, the cell layer was scratched along the line drawn on the back of the plate the day before. After the scratch was completed, cells were washed three times with PBS, and fresh serum-free medium was replaced. Cells were cultured in an incubator at 37°C with 5% CO_2. Cells were removed at 0 h and 24 h, and the area of the scratch was observed and measured under a microscope. Cell migration was calculated using the formula: Cell migration rate = 1 − (scratch area at 24 h/scratch area at 0 h). Two-tailed *t*-tests were used to compare the results of different groups, and data are presented as the mean ± SEM. We used Graphpad Prism 9.0 to visualize the data.

Data availability

Supplementary material is available at figshare: https://doi.org/10.25387/g3.14058293.

Supplementary Table S1: miRNA-Seq date. The miRNA expression data for each sample was normalized using the TPM method.

Supplementary Table S2: GO and KEGG enrichment analyses.

Results

Differential expression of miRNAs

To identify miRNAs associated with the initiation of PC and DC formation, differential expression of miRNAs at three stages (45, 55, and 65 days) was analyzed. Comparison between 55 days and 45 days revealed 466 differentially expressed miRNAs (188 upregulated and 278 downregulated at 55 days), and 35 miRNAs had TPM values >1000 and a *P*-value of <0.05 (Figure 1A). Comparison between 55 days and 65 days revealed 464 differentially expressed miRNAs (317 upregulated and 147 downregulated, of which 25 miRNAs had TPM values >1000 and *P*-values <0.05 (Figure 1B). Comparing miRNAs upregulated at 55 days and TPM values >1000 revealed 17 overlapping candidate miRNAs (Figure 1C). Expression levels of all miRNAs at three stages were measured and normalized by TPM, and the fold-change (FC) of candidate miRNAs in the two groups was calculated and normalized by $\log_2$ (FC).

Screening of miRNAs associated with PC and DC morphogenesis

For mRNA data, functional analysis is typically conducted using GO and KEGG enrichment analyses (Supplementary Table S2), while for miRNA data, miRNA-related functions are usually studied through corresponding mRNAs. Analysis of candidate miRNAs using TargetScan and MiRanda predicted 22,731 target genes. The results of GO functional analysis showed that candidate miRNAs were mainly associated with intracellular and cytoplasm in the cellular component category, binding and protein binding the molecular function category, and positive regulation

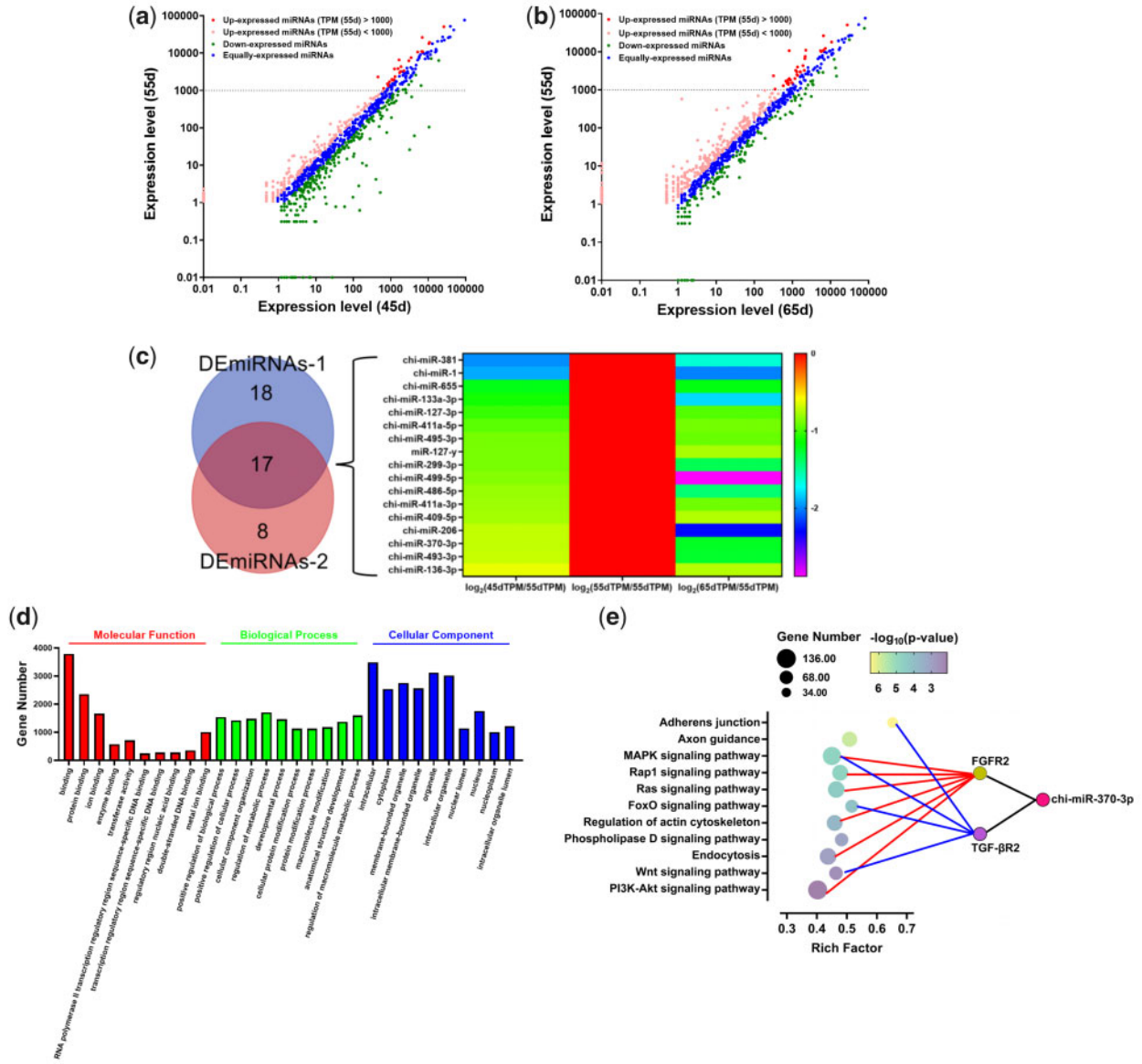

Figure 1 Screening of miRNAs related to fetal skin hair follicle morphogenesis in Inner Mongolian cashmere goats. (A) miRNAs differentially expressed at 55 and 45 days. (B) miRNAs differentially expressed at 55 and 65 days. (C) Heatmap of miRNAs related to DC and PC initiation. (D) GO functional annotation and enrichment analysis. The top 10 GO terms in each category are shown in the figure. (E) KEGG signaling pathway enrichment analysis.

of biological processes and cellular processes in the biological process category (Figure 1D).

Compared with GO functional enrichment analysis, we paid more attention to the results of KEGG signaling pathway enrichment analysis, since this identified 35 signaling pathways in which candidate miRNAs were significantly enriched, 11 of which were involved in the initiation of PC and DC formation (Figure 1E). We found that chi-miR-370-3p was enriched in nine signaling pathways through targeting *TGF-βR2* and *FGFR2*. These results suggest that chi-miR-370-3p may affect the initiation of PC and DC formation by regulating *TGF-βR2* and *FGFR2* (Figure 1E). Since the miRNA sequencing results were verified by qRT-PCR in previous work (Han *et al.* 2020), we focused only on chi-miR-370-3p in the present work, and relative expression levels of chi-miR-370-3p were consistent with the RNA-seq results (Figure 2A).

Chi-miR-370-3p targets *TGF-βR2* and *FGFR2*

qRT-PCR results showed that the relative expression levels of *TGF-βR2* and *FGFR2* were strongly negatively correlated with chi-miR-370-3p at 45–65 days, with Pearson product–moment correlation coefficient of −0.95833 and −0.88787, respectively (Figure 2B). Sequence alignment of chi-miR-370-3p with *FGFR2* and *TGF-βR2* revealed that chi-miR-370-3p possessed binding sites for TGF-βR2-3′-UTR and FGFR2-3′-UTR, and *TGF-βR2* and *FGFR2* were confirmed as potential target genes of chi-miR-370-3p (Figure 2C). Finally, chi-miR-130b-3p significantly downregulated the expression of the wild-type TGF-βR2-3′-UTR (Figure 2D) and FGFR2-3′-UTR (Figure 2E), according to the results of the dual-luciferase reporter gene assay system ($P < 0.01$), indicating binding between the two molecules, and this downregulation effect disappeared after mutation ($P > 0.05$), indicating that the mutation was successful (Figure 2, D and E).

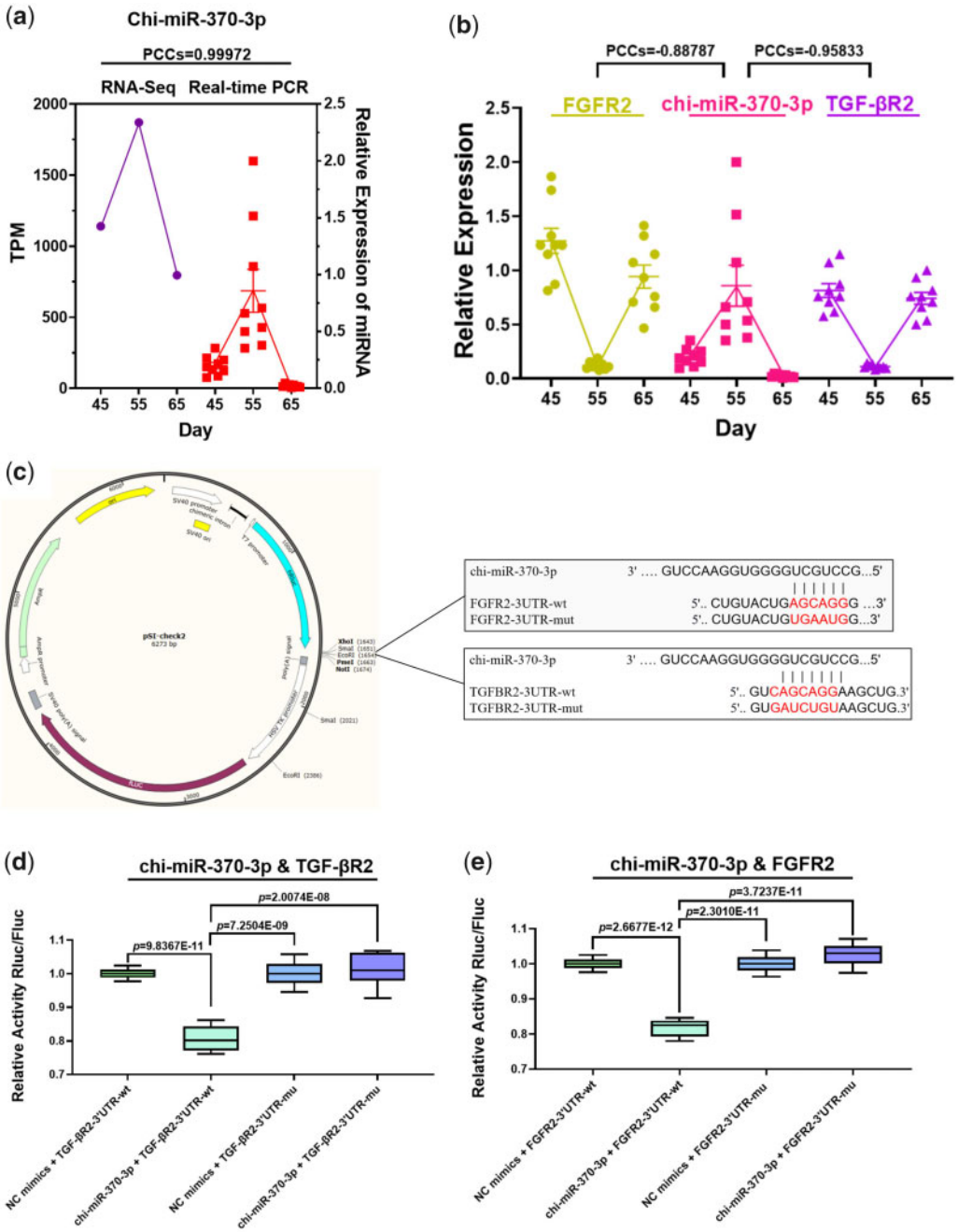

Figure 2 Verification of chi-miR-370-3p sequencing results and confirmation that it directly targets *TGF-βR2* and *FGFR2*. (A) Validation of chi-miR-370-3p sequencing results. (B) qRT-PCR verification of the targeting of *TGF-βR2* and *FGFR2* by chi-miR-370-3p. (C) Plasmid map of the dual luciferase reporter system and location of the target fragment inserted into the vector. (D) Verification of the interaction between chi-miR-370-3p and TGF-βR2-3′-UTR by dual luciferase reporter gene assay. (E) Verification of the interaction between chi-miR-370-3p and FGFR2-3′-UTR by dual luciferase reporter gene assay.

Functions of chi-miR-370-3p in epithelial cells and dermal fibroblasts

After puromycin resistance screening, fluorescence microscopy showed that resistance screening was successful; both dermal fibroblasts and epithelial cells exhibited strong green fluorescence with a uniform distribution (Figure 3A). The qRT-PCR results showed that the relative expression of chi-miR-370-3p in the chi-miR-370-3p (lo) group was significantly lower than that in the NC group ($P < 0.01$), while that in the chi-miR-370-3p (hi) group was significantly higher than that in the NC group ($P < 0.01$), both in epithelial cells and in dermal fibroblasts (Figure 3B). This confirmed that both chi-miR-370 (lo) and chi-miR-370 (hi) epithelial cell and dermal fibroblast lines were constructed successfully.

The qRT-PCR results showed that in each epithelial cell line, expression of *TGF-βR2* in the chi-miR-370(lo) group was 5.08672 times higher than that in the NC group ($P < 0.01$), while expression of *FGFR2* in the chi-miR-370 (lo) group was 5.56757 times higher than that in the NC group ($P < 0.01$). Expression of *TGF-βR2* in the chi-miR-370 (hi) group was 0.19037 times higher than that in the NC group ($P < 0.01$), and expression of *FGFR2* in the chi-miR-370 (hi) group was 0.10153 times higher than that in the

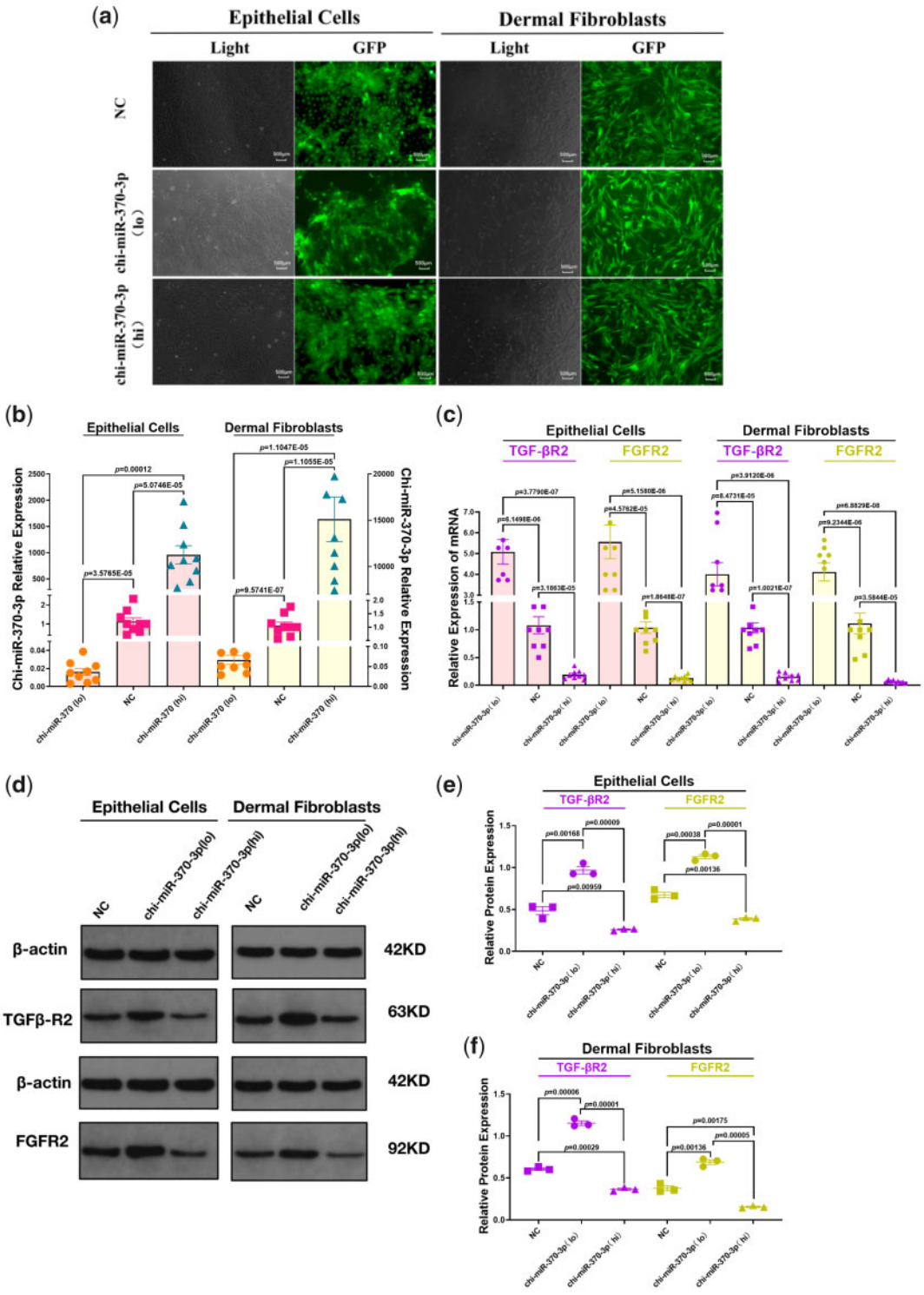

Figure 3 Verification of the regulatory effect of chi-mir-370-3p on TGF-βR2 and FGFR2 at epithelial cell and dermal fibroblast levels. (A) Construction of chi-miR-370-3p (lo) and chi-miR-370-3p (hi) dermal fibroblast and epithelial cell lines. (B) Relative expression of chi-miR-370-3p in various cell lines. (C) Relative expression of *TGF-βR2* and *FGFR2* in various cell lines. (D) Expression of β-actin, TGF-βR2, and FGFR2 proteins in each cell line. (E) Relative abundance of TGF-βR2 and FGFR2 proteins in different epithelial cell lines. (F) Relative abundance of TGF-βR2 and FGFR2 proteins in different dermal fibroblast cell lines.

NC group ($P < 0.01$). In each dermal fibroblast line, expression of *TGF-βR2* in the chi-miR-370 (lo) group was 4.01207 times higher than that in the NC group ($P < 0.01$), while expression of *FGFR2* in the chi-miR-370 (lo) group was 4.11829 times higher than that in the NC group ($P < 0.01$). Expression of *TGF-βR2* in the chi-miR-370 (hi) group was 0.15207 times higher than that in the NC group ($P < 0.01$), and expression of *FGFR2* in the chi-miR-370 (hi) group was 0.06429 times higher than that in the NC group ($P < 0.01$; Figure 3C).

Western blotting results analyzed by Image-Pro Plus yielded gray values for TGF-βR2, FGFR2, and β-actin for each treatment

group of epithelial cells and dermal fibroblasts, and the relative expression of TGF-βR2 and FGFR2 protein in each experimental group of epithelial cells and dermal fibroblasts (Figure 3D). In epithelial cells, TGF-βR2/β-actin values for NC, chi-miR-370-3p (lo), and chi-miR-370-3p (hi) groups were 0.48522, 0.96745, and 0.26001, respectively. FGFR2/β-actin values for NC, chi-miR-370-3p (lo), and chi-miR-370-3p (hi) groups were 0.67359, 1.12867, and 0.36017, respectively (Figure 3E). In dermal fibroblasts, TGF-βR2/β-actin values for NC, chi-miR-370-3p (lo), and chi-miR-370-3p (hi) groups were 0.60533, 1.15414, and 0.38776, respectively. FGFR2/β-actin values for NC, chi-miR-370-3p (lo), and chi-miR-370-3p (hi) groups were 0.37655, 0.72622, and 0.17165, respectively (Figure 3F). These results confirmed that chi-miR-370-3p negatively regulates both *TGF-βR2* and *FGFR2* genes during hair follicle development in goat fetal skin.

Effects of chi-miR-370-3p on the cell cycle, proliferation, apoptosis, and migration of epithelial cells and dermal fibroblasts

DNA staining results (Figure 4A) showed that with increasing expression of chi-miR-370-3p in epithelial cells, the proportion of cells in phase G0/G1 of the cell cycle was significantly increased

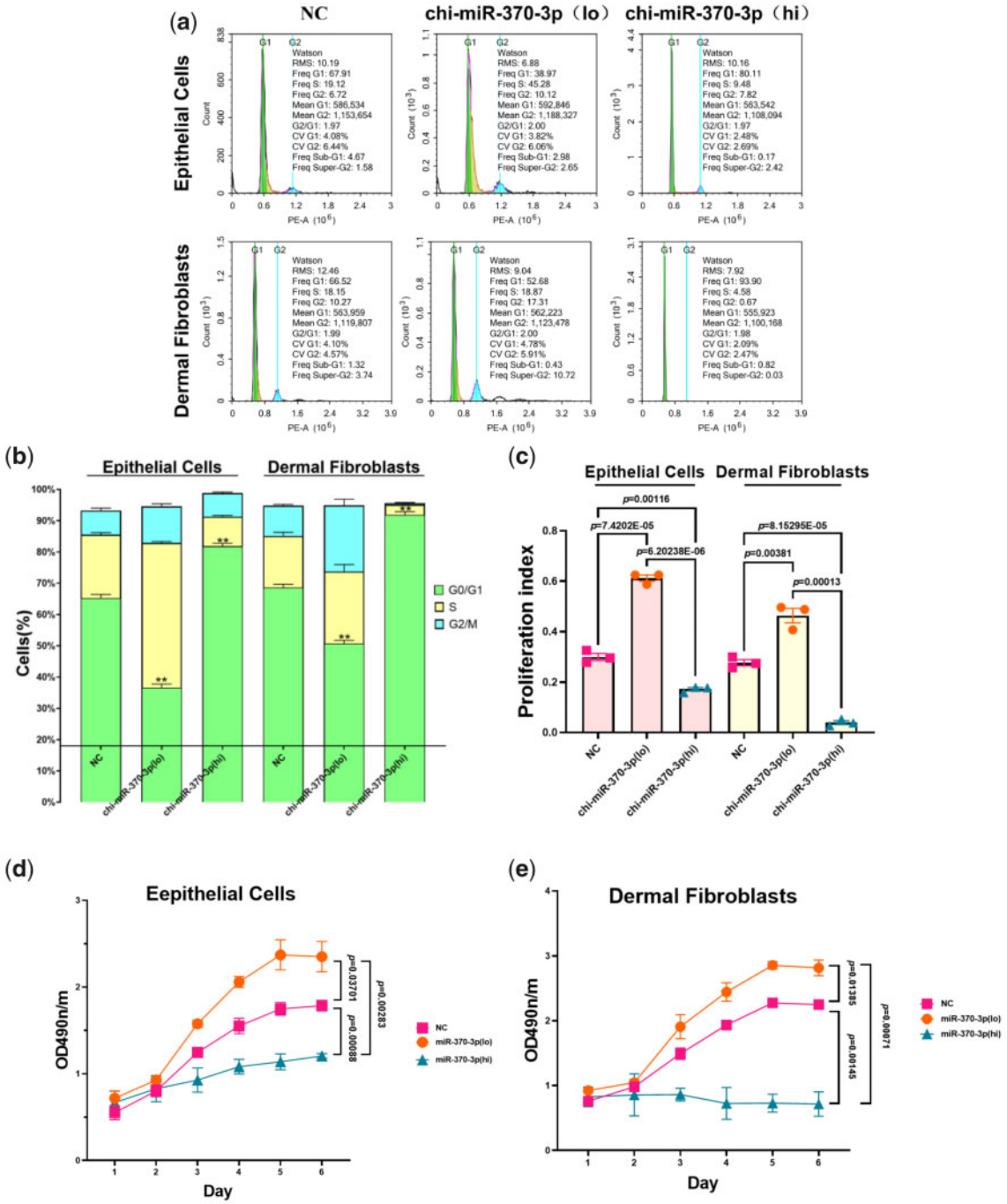

Figure 4 Effects of chi-miR-370-3p on the proliferation of epithelial cells and dermal fibroblasts. (A) Cell cycle analysis by flow cytometry. (B) Statistical analysis of the cell cycle in each cell line (**$P < 0.01$). (C) Increment index of each cell line. (D) Cell growth curve for each epithelial cell line. (E) Cell growth curve for each dermal fibroblast cell line.

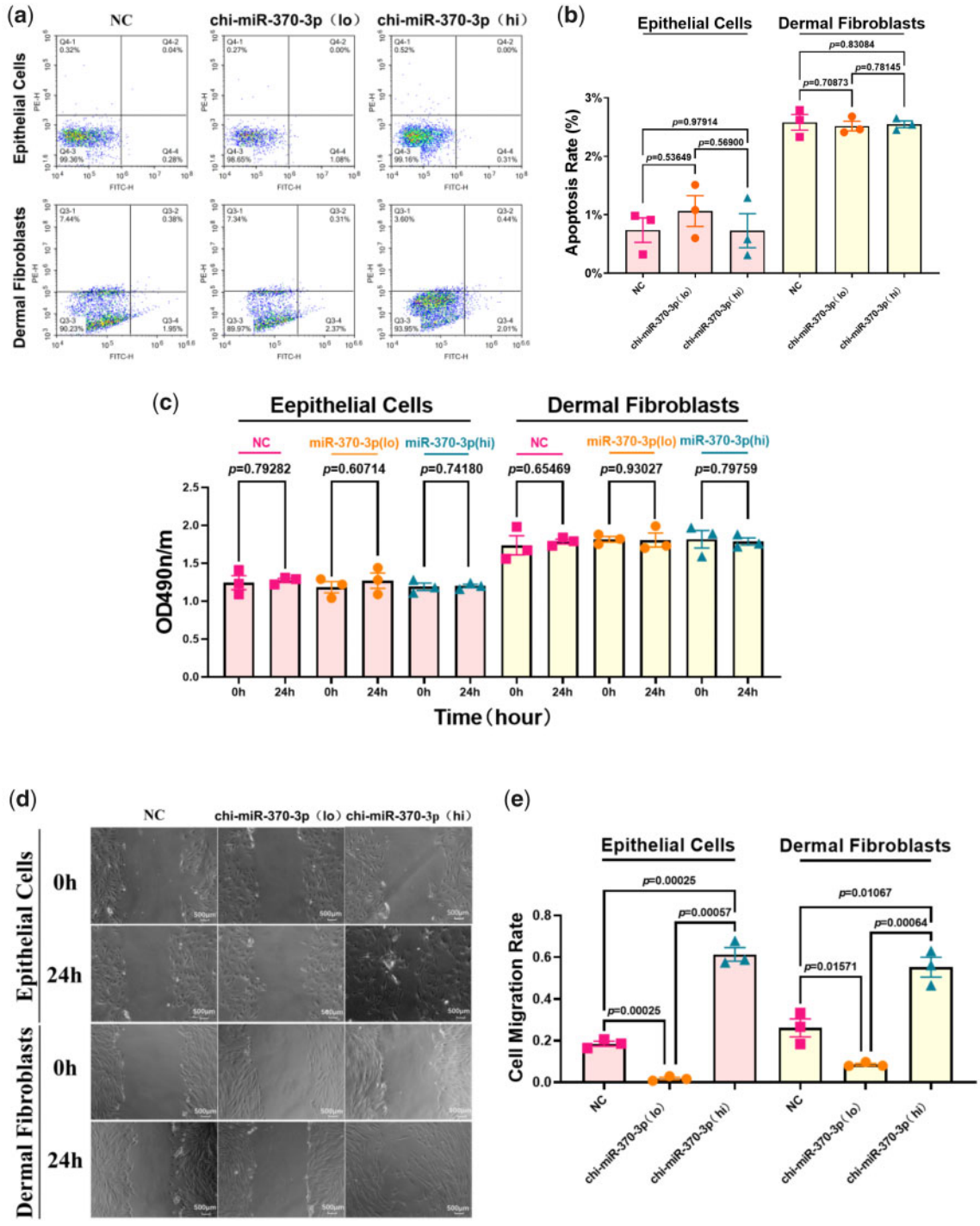

Figure 5 Effects of chi-miR-370-3p on apoptosis and migration of epithelial cells and dermal fibroblasts. (A) Apoptosis analysis by flow cytometry. (B) Apoptosis rate of each cell line. (C) Effect of serum-free medium on the proliferation of each cell line over 24 h. (D) Results of cell scratch tests. (E) Cell migration rate of each cell line.

(Figure 4B), and the cell proliferation rate was significantly decreased (Figure 4C). Similarly, in dermal fibroblasts, with increasing expression of chi-miR-370-3p, the proportion of cells in phase G0/G1 of the cell cycle was significantly increased (Figure 4B), and the cell proliferation rate was significantly decreased (Figure 4C).

CCK-8 assay results showed that with increasing expression of chi-miR-370-3p in epithelial cells (Figure 4D) and dermal fibroblasts (Figure 4E), cell proliferation was significantly reduced ($P < 0.01$). The fluorescein-labelled Annexin V results (Figure 5A) showed that epithelial cells and fibroblasts did not undergo significant changes in apoptosis with different expression levels of chi-miR-370-3p ($P > 0.05$; Figure 5B).

We cultured cells in serum-free medium to reduce the effect of cell proliferation in the cell scratch experiment. The CCK-8 results showed no significant changes in cell proliferation in each epithelial and dermal fibroblast cell line in serum-free medium for 24 h ($P > 0.05$; Figure 5C). The cell scratch test results

(Figure 5D) showed that in epithelial cells, the cell migration rate of the chi-miR-370-3p (lo) group was significantly lower than that of the NC group ($P < 0.01$) after 24 h, and the cell migration rate of the chi-miR-370-3p (hi) group was significantly higher than that of the NC group ($P < 0.01$) after 24 h. Meanwhile, in dermal fibroblasts, the cell migration rate of the chi-miR-370-3p (lo) group was significantly lower than that of the NC group ($P < 0.01$) after 24 h, and the cell migration rate of the chi-miR-370-3p (hi) group was significantly higher than that of the NC group ($P < 0.01$) after 2 h (Figure 5E). Thus, chi-miR-370-3p can stimulate the migration of both epithelial cells and dermal fibroblasts.

Discussion

The morphogenesis of hair follicles is coordinated by interactions between epithelium (epidermis) and mesenchyma (dermis) (Sengel 1990). Epithelial cells that form the epidermis receive signals from the underlying dermal fibroblasts to form the PC, while dermal fibroblasts require epidermal signals to form DC (Davidson and Hardy 1952; Hardy 1992; Kollar 1970). PC morphogenesis is stimulated by the activation of the nuclear factor κ-light-chain-enhancer of activated B cells and WNT signaling pathways, which can enhance the motility of epithelial cells and increase the abundance of epithelial cells needed to form the PC (Ahtiainen *et al.* 2014). In the process through which epithelial cells form the PC, PC precursors release Wnt family and other signaling molecules that are received by dermal fibroblasts, and dermal fibroblasts subsequently determine the cell fate of directed aggregation (Mok *et al.* 2019). It is known that PC and DC formation depends on cell migration rather than cell proliferation, but changes in fate determination of epithelial cells and fibroblasts may be related to the control of cell proliferation (Ahtiainen *et al.* 2014; Mok *et al.* 2019). Cell proliferation is an important process through which epithelial cells form a complete epidermis. At this stage, a large number of signal molecules related to cell proliferation are active, including members of the TGF-β and FGF family. Members of the TGF-β family are considered crucial for hair follicle formation, but *TGF-βR2* is usually only expressed in the epidermal structure before the formation of the PC (Paus *et al.* 1997). *FGFR2*-deficient mice can exhibit severe epidermal dysplasia (Petiot *et al.* 2003). Increasing the expression of *FGFR2* can induce epithelial cells to differentiate into epidermis, but it can increase the duration of hair follicle formation and reduce the number of hair follicle units (Richardson *et al.* 2009). High expression of *FGF7* can also inhibit the formation of hair follicles (Guo *et al.* 1993). Compared with epithelial cells that form the PC, the dermal fibroblasts that form DC almost exit the cell cycle, resulting in almost the complete loss of proliferation ability (Mok *et al.* 2019), suggesting that the migration ability acquired by epithelial and dermal fibroblasts to form PC and DC is likely to be associated with inhibition of cell proliferation (Magerl *et al.* 2001; Richardson *et al.* 2009; Schmidt-Ullrich *et al.* 2006).

MiRNAs target regulatory genes and form a diverse regulatory network during the development of skin hair follicles. They also play a key role in gene expression in different cell lines of hair follicles. In the Wnt/β-catenin signaling pathway, miR-214 targets *β-catenin* to inhibit the Wnt signaling pathway, which affects the proliferation of epithelial cells and decreases hair formation (Amelio *et al.* 2013). miR-218-5p is a dynamic regulator of hair follicle development that targets *secreted frizzled related protein 2* to activate the Wnt/β-catenin signaling pathway (Zhao *et al.* 2019). This miRNA not only plays a role in this signaling pathway; *keratin 16*, *keratin 17*, *distal-less homeobox 3*, and *FGF10* are also direct targets miR-31, and overexpression and deletion of miR-31 affect the activity of both bone morphogenetic protein (BMP) and WNT signaling pathways (Mardaryev *et al.* 2010).

The Let-7 family is one of the most abundant miRNA families in epidermal cells (Rybak *et al.* 2009), and members mediate the transformation of undifferentiated basal cells to basalization (Bussing *et al.* 2008). Let-7a targets *insulin-like growth factor 1 receptor*, *transcriptional regulator Myc-like*, and *FGF5*, regulating their corresponding signaling pathways and thereby affecting the development of hair follicles (Ma *et al.* 2018). Hairless mouse mutants exhibit altered *TGF-β2* expression through miR-31 regulation, which interferes with hair follicle morphogenesis and hair circulation (Kim and Yoon 2015). The BMP signaling pathway is important in epithelial cells and plays an important role in fetal post-birth tissue remodeling and tumorigenesis. miR-21 and *inhibitor of DNA binding 1*, *inhibitor of DNA binding 2*, *inhibitor of DNA binding 3*, and *msh homeobox 2* are important downstream components of the BMP signaling pathway (Ahmed *et al.* 2011). Alopecia areata is one of the most common types of alopecia in humans (Jabbari *et al.* 2018; Liu *et al.* 2017; Pratt *et al.* 2017; Rajabi *et al.* 2018; Strazzulla *et al.* 2018a, 2018b; Trüeb and Dias 2018). Risk-associated genes *interleukin 2 receptor subunit alpha* (*IL2RA*), *syntaxin 17* (*STX17*), and *tenascin XB* (*TNXB*) are regulated by miR-30b, and low expression of miR-30b in alopecia areata patients leads to increased expression of *IL2RA*, *STX17*, and *TNXB*, which greatly increases the probability of disease (Tafazzoli *et al.* 2018). In addition, four kinds of differentially expressed miRNAs were identified in dermal papilla cells with and without alopecia (Goodarzi *et al.* 2012). As a rare hereditary hair disease, alopecia–neurological defects–endocrinopathy syndrome is caused by decreased expression of *RNA-binding motif protein 28*, which promotes hair growth by regulating the activities of miR-203 and the coding transcription factor p63 (Warshauer *et al.* 2015).

In the present study, we demonstrated that chi-miR-370-3p can increase the proportion of epithelial cells and dermal fibroblasts at the G0/G1 stage and inhibit cell proliferation by regulating *TGF-βR2* and *FGFR2* expression at mRNA and protein levels, thereby stimulating cell migration. We revealed a relationship between cell migration and cell proliferation during hair follicle morphogenesis and showed that inhibition of the expression of certain proliferation-related genes by miRNAs may be the key to enhancing the migration ability of epithelial cells and dermal fibroblasts.

Conclusion

Chi-miR-370-3p is a key miRNA in the morphogenesis of fetal hair follicles of Inner Mongolian cashmere goats. This miRNA inhibits the proliferation of epithelial cells and dermal fibroblasts through targeted regulation of *FGFR2* and *TGF-βR2*, thereby promoting their migration ability, and this process does not increase cell apoptosis.

Ethics approval and consent to participate

All fetal skin samples were collected in accordance with the International Guiding Principles for Biomedical Research Involving Animals and approved by the Special Committee on Scientific Research and Academic Ethics of Inner Mongolia Agricultural University, responsible for the approval of biomedical research ethics of Inner Mongolia Agricultural University (Approval No. [2020] 056). No specific permissions were required

for these activities, and no endangered or protected species were involved.

Acknowledgments

The authors thank International Science Editing (http://www.internationalscienceediting.com) for editing an earlier version of this article (January 25, 2021). The authors thank the Inner Mongolia Jinlai Animal Husbandry Technology Co., Ltd.

Funding

This research was funded by the National Natural Science Foundation of China (31860627) and the Plan Project of Science and Technology in Inner Mongolia (2019GG243).

Conflict of interest: None declared.

Literature cited

Ahtiainen L, Lefebvre S, Lindfors PH, Elodie R, Vera S, *et al.* 2014. Directional cell migration, but not proliferation, drives hair placode morphogenesis. Dev Cell. 28:588–602.

Andl T, Murchison EP, Liu F, Zhang Y, Yunta-Gonzalez M, *et al.* 2006. The microRNA-processing enzyme dicer is essential for the morphogenesis and maintenance of hair follicles. Curr Biol. 16: 1041–1049.

Ahmed MI, Alam M, Emelianov VU, Poterlowicz K, Patel A, *et al.* 2014. MicroRNA-214 controls skin and hair follicle development by modulating the activity of the Wnt pathway. J Cell Biol. 207: 549–567.

Amelio I, Lena AM, Bonanno E, Melino G, Candi E. 2013. miR-24 affects hair follicle morphogenesis targeting Tcf-3. Cell Death Dis. 4:e922.

Ahmed MI, Mardaryev AN, Lewis CJ, Sharov AA, Botchkareva NV. 2011. MicroRNA-21 is an important downstream component of BMP signalling in epidermal keratinocytes. J Cell Sci. 124: 3399–3404.

Bussing I, Slack FJ, Grosshans H. 2008. let-7 microRNAs in development, stem cells and cancer. Trends Mol Med. 14:400–409.

Bruce W, Iiho H, Gary R. 1993. Posttranscriptional regulation of the heterochronic gene lin-14 by lin-4 mediates temporal pattern formation in *C. elegans*. Cell. 75:855–862.

Bartel DP. 2018. Metazoan microRNAs. Cell. 173:20–51.

Davidson P, Hardy MH. 1952. The development of mouse vibrissae in vivo and in vitro. J Anat. 86:342–356.

Epstein FH, Paus R, Cotsarelis G. 1999. The biology of hair follicles. N Engl J Med. 341:491–497.

Goodarzi HR, Abbasi A, Saffari M, Fazelzadeh Haghighi M, Tabei MB, *et al.* 2012. Differential expression analysis of balding and non-balding dermal papilla microRNAs in male pattern baldness with a microRNA amplification profiling method. Br J Dermatol. 166: 1010–1016.

Gao Y, Wang XL, Yan HL, Zen J, Ma S, *et al.* 2016. Comparative transcriptome analysis of fetal skin reveals key genes related to hair follicle morphogenesis in cashmere goats. PLoS One. 11: e0151118.

Guo L, Yu Q, Fuchs E. 1993. Targeting expression of keratinocyte growth factor to keratinocytes elicits striking changes in epithelial differentiation in transgenic mice. Embo J. 12:973–986.

Gebert LFR, Macrae IJ. 2019. Regulation of microRNA function in animals. Nat Rev Mol Cell Biol. 20:21–37.

Hardy MH. 1992. The secret life of the hair follicle. Trends Genet. 8: 55–61.

Han WJ, Yang F, Wu ZH, Guo FQ, Zhang JJ, *et al.* 2020. Inner mongolian cashmere goat secondary follicle development regulation research based on mRNA-miRNA co-analysis. Sci Rep. 10:4519.

Jabbari A, Sansaricq F, Cerise J, Chen JC, Bitterman A, *et al.* 2018. An open-label pilot study to evaluate the efficacy of tofacitinib in moderate to severe patch-type alopecia areata, totalis, and universalis. J Invest Dermatol. 138:1539–1545.

Kozomara A, Birgaoanu M, Griffiths-Jones S. 2019. miRBase: from microRNA sequences to function. Nuc Acids Res. 47:155–162.

Kim BK, Yoon SK. 2015. Hairless up-regulates Tgf-β2 expression via down-regulation of miR-31 in the skin of "Hairpoor" (HrHp) mice. J Cell Physiol. 230:2075–2085.

Kollar EJ. 1970. The induction of hair follicles by embryonic dermal papillae. J Invest Dermatol. 55:374–378.

Liu H, Yu H, Tang G, Huang T. 2018. Small but powerful: function of microRNAs in plant development. Plant Cell Rep. 37:515–528.

Lee RC, Rhonda LF, Victor A. 1993. The *C. elegans* heterochronic gene lin-4 encodes small RNAs with antisense complementarity to lin-14. Cell. 75:843–854.

Liu LY, Craiglow BG, Dai F, King BA. 2017. Tofacitinib for the treatment of severe alopecia areata and variants: a study of 90 patients. J Am Acad Dermatol. 76:22–28.

Ma T, Li JP, Jiang Q, Wu SF, Jiang HZ, *et al.* 2018. Differential expression of miR-let7a in hair follicle cycle of Liaoning cashmere goats and identification of its targets. Funct Integr Genomics. 18: 701–707.

Mardaryev AN, Ahmed MI, Vlahov NV, Fessing MY, Gill JH, *et al.* 2010. MicroRNA-31 controls hair cycle-associated changes in gene expression programs of the skin and hair follicle. Faseb J. 24: 3869–3881.

Mok KW, Saxena N, Heitman N, Grisanti L, Srivastava D, *et al.* 2019. dermal condensate niche fate specification occurs prior to formation and is placode progenitor dependent. Dev Cell. 48:32–48.

Magerl M, Tobin DJ, Müller-Röver S, Hagen E, Lindner G, *et al.* 2001. Patterns of proliferation and apoptosis during murine hair follicle morphogenesis. J Invest Dermatol. 116:947–955.

Pratt CH, King LE, Messenger AG, Christiano AM, Sundberg PE. 2017. Alopecia areata. N Engl J Med. 3:17011.

Paus R, Foitzik K, Welker P, Bulfone-Paus S, Eichmüller S. 1997. Transforming growth factor-beta receptor type I and type II expression during murine hair follicle development and cycling. J Invest Dermatol. 109:518–526.

Petiot A, Conti FJ, Grose R, Revest JM, Hodivala-Dilke KM, *et al.* 2003. A crucial role for Fgfr2-IIIb signalling in epidermal development and hair follicle patterning. Development. 130:5493–5501.

Rajabi F, Drake LA, Senna MM, Rezaei N. 2018. Alopecia areata: a review of disease pathogenesis. Br J Dermatol. 179:1033–1048.

Rybak A, Fuchs H, Hadian K, Smirnova L, Wulczyn EA, *et al.* 2009. The let-7 target gene mouse lin-41 is a stem cell specific E3 ubiquitin ligase for the microRNA pathway protein Ago2. Nat Cell Biol. 11:1411–1420.

Richardson GD, Bazzi H, Fantauzzo KA, Waters JM, Crawford H, *et al.* 2009. KGF and EGF signalling block hair follicle induction and promote interfollicular epidermal fate in developing mouse skin. Development. 136:2153–2164.

Shamsaddini-Bafti M, Salehi M, Maghsoudi A, Tehrani AM, Mirzaei F, *et al.* 2012. Effect of sex and rearing system on the quality and mineral content of fiber from raeini cashmere goats. J Anim Sci Biotechnol. 3:20.

Suzuki HI, Katsura A, Yasuda T, Ueno T, Mano H, *et al.* 2015. Small-RNA asymmetry is directly driven by mammalian Argonautes. Nat Struct Mol Biol. 22:512–521.

Schmittgen TD, Livak KJ. 2008. Analyzing real-time PCR data by the comparative CT method. Nat Protoc. 3:1101–1108.

Sengel P. 1990. Pattern formation in skin development. Int J Dev Biol. 34:33–50.

Schmidt-Ullrich R, Tobin DJ, Lenhard D, Schneider P, Paus R, *et al.* 2006. NF-kappaB transmits Eda A1/EdaR signalling to activate Shh and cyclin D1 expression, and controls post-initiation hair placode down growth. Development. 133:1045–1057.

Strazzulla LC, Wang EHC, Avila L, Lo SK, Brinster N, *et al.* 2018a. Alopecia areata: disease characteristics, clinical evaluation, and new perspectives on pathogenesis. J Am Acad Dermatol. 78:1–12.

Strazzulla LC, Wang EHC, Avila L, Lo SK, Brinster N, *et al.* 2018b. Alopecia areata: an appraisal of new treatment approaches and overview of current therapies. J Am Acad Dermatol. 78:15–24.

Trüeb RM, Dias MFRG. 2018. Alopecia areata: a comprehensive review of pathogenesis and management. Clin Rev Allergy Immunol. 54:68–87.

Tafazzoli A, Forstner AJ, Broadley D, Hofmann A, Redler S, *et al.* 2018. Genome-wide MicroRNA analysis implicates miR-30b/d in the etiology of alopecia areata. J Invest Dermatol. 138:549–556.

Wu ZH, Hai EH, Di ZY, Ma R, Shang FZ, *et al.* 2020a. Using WGCNA (weighted gene co-expression network analysis) to identify the hub genes of skin hair follicle development in fetus stage of Inner Mongolia cashmere goat. PLoS One. 15:e0243507.

Wu ZH, Wang Y, Han WJ, Yang K, Hai EH, *et al.* 2020b. EDA and EDAR expression at different stages of hair follicle development in cashmere goats and effects on expression of related genes. Arch Anim Breed. 63:461–470.

Wang SH, Li F, Liu JW, Zhang YL, Zheng YJ, *et al.* 2020. Integrative analysis of methylome and transcriptome reveals the regulatory mechanisms of hair follicle morphogenesis in cashmere goat. Cells. 9:969.

Wu ZH, Hai EH, Di ZY, Ma R, Shang FZ, *et al.* 2021. Chi-miR-130b-3p regulates Inner Mongolia cashmere goat skin hair follicles in fetuses by targeting Wnt family member 10A. G3 (Bethesda). 11:1–8.

Warshauer E, Samuelov L, Sarig O, Vodo D, Bindereif A, *et al.* 2015. RBM28, a protein deficient in ANE syndrome, regulates hair follicle growth via miR-203 and p63. Exp Dermatol. 24:618–622.

Yi R, O'Carroll D, Pasolli HA, Zhang ZH, Dietrich FS, *et al.* 2006. Morphogenesis in skin is governed by discrete sets of differentially expressed microRNAs. Nat Genet. 38:356–362.

Yi R, Pasolli HA, Landthaler M, Hafner M, Ojo T, *et al.* 2009. DGCR8-dependent microRNA biogenesis is essential for skin development. Proc Natl Acad Sci U S A. 106:498–502.

Zhang YJ, Wang LL, Li Z, Chen D, Han WJ, *et al.* 2019. Transcriptome profiling reveals transcriptional and alternative splicing regulation in the early embryonic development of hair follicles in the cashmere goat. Sci Rep. 9:17735.

Zhao BH, Chen Y, Yang NS, Chen QR, Bao ZY, *et al.* 2019. miR-218-5p regulates skin and hair follicle development through Wnt/β-catenin signaling pathway by targeting SFRP2. J Cell Physiol. 234:20329–20341.

Communicating editor: J. Birchler